Inorg. Chem. **2003**, *42*, 2261–2267

Verdazyl Radicals as Oligopyridine Mimics: Structures and Magnetic Properties of M(II) Complexes of 1,5-Dimethyl-3-(2,2′-bipyridin-6-yl)-6-oxoverdazyl (M = Mn, Ni, Cu, Zn)

Tosha M. Barclay,[†] Robin G. Hicks,*[,‡] Martin T. Lemaire,[‡] and Laurence K. Thompson[§]

Departments of Chemistry, Mississippi State University, Box 9573, State College, Mississippi 39762, University of Victoria, P.O. Box 3065, Victoria, British Columbia V8W 3V6, Canada, and Memorial University of Newfoundland, St. John's, Newfoundland A1B 3X7, Canada

Received August 19, 2002

The verdazyl radical 1,5-dimethyl-3-(2,2′-bipyridin-6-yl)-6-oxoverdazyl (**3**) was prepared, and its homoleptic metal complexes $M(\mathbf{3})_2^{2+}\cdot 2X^-$ (**5**, M = Mn(II); **6**, M = Ni(II); **7**, M = Cu(II); **8**, M = Zn(II); X = ClO_4, PF_6) were characterized by single-crystal X-ray diffraction and variable-temperature magnetic susceptibility measurements. Relevant crystallographic parameters are as follows: **5**, monoclinic space group $Pna2_1$, a = 18.755(4) Å, b = 11.154(3) Å, c = 16.594(4) Å, α = 90.00°, β = 90.00°, γ = 90.00°, V = 3471.4(13) Å^3, and Z = 4; **7**, triclinic space group $P\bar{1}$, a = 9.4638(18) Å, b = 9.8442(19) Å, c = 18.769(4) Å, α = 103.746(3)°, β = 92.925(3)°, γ = 94.869(3)°, V = 1687.8(6) Å^3, and Z = 2; **8**, triclinic space group $P\bar{1}$, a = 9.4858(14) Å, b = 9.7919(14) Å, c = 18.889(3) Å, α = 104.196(3)°, β = 92.855(3)°, γ = 94.216(3)°, V = 1692.1(4) Å^3, and Z = 2. In all cases, the two verdazyl-based ligands bind almost perpendicular to each other in meridional positions, yielding pseudooctahedral metal complexes whose general structural features are strongly reminiscent of metal bis(terpyridine) complexes. The intramolecular metal–verdazyl magnetic exchange coupling is strongly ferromagnetic in **6** (J_{Ni-vd} = +240 cm^{-1}), and strongly antiferromagnetic in **5** (J_{Mn-vd} = –93 cm^{-1}). Complex **7** exhibits weak ferromagnetic coupling (J_{Cu-vd} = –4.5 cm^{-1}). Intramolecular radical–radical coupling in the zinc complex **8** was found to be weakly antiferromagnetic (J_{vd-vd} = –8 cm^{-1}). Intramolecular radical–radical exchange was generally weak in the four metal complexes, ranging from –10 cm^{-1} (for **5**) to +2 cm^{-1} (for **7**). The low-temperature magnetic behavior of **7** and **8** is complex, possibly arising from a combination of intra- and intermolecular interactions.

Introduction

The coordination chemistry of spin-bearing ligands has received considerable attention in the quest for new molecule-based magnetic materials.[1,2] The primary advantage of the "metal−radical approach" is that direct exchange interactions between the metal−radical pair can provide stronger coupling than in the superexchange mechanism, in which coupling between metals is transmitted through a diamagnetic bridging ligand. Discrete molecular transition-metal complexes containing open shell ligands, though not themselves candidates as magnetic materials, are useful as models for the magnetic exchange coupling expected in extended structures of higher lattice dimensionality.

Current families of radicals that have been extensively studied in this regard include neutral radicals such as nitroxides (including nitronyl nitroxides and imino nitroxides),[2,3] as well as radical anions, including semiquinones[4] and cyanocarbon acceptors such as tcne.[5] In recent years coordination complexes of other kinds of stable radicals have begun to be explored.[6] Recent work by us and others has shown that judiciously substituted verdazyl[7] radicals such

* Author to whom correspondence should be addressed. E-mail: rhicks@uvic.ca.
[†] Mississippi State University.
[‡] University of Victoria.
[§] Memorial University of Newfoundland.

(1) Caneschi, A.; Gatteschi, D.; Sessoli, R. *Acc. Chem. Res.* **1989**, *22*, 392.
(2) Caneschi, A.; Gatteschi, D.; Rey, P. *Prog. Inorg. Chem.* **1991**, *39*, 331.
(3) (a) Stumph, H. O.; Ouahab, L.; Pei, Y.; Grandjean, D.; Kahn, O. *Science* **1993**, *261*, 447. (b) Inoue, K.; Hayamizu, T.; Iwamura, H.; Hashizume, D.; Ohashi, Y. *J. Am. Chem. Soc.* **1996**, *118*, 1803.
(4) (a) Pierpont, C. G.; Lange, C. W. *Prog. Inorg. Chem.* **1994**, *41*, 331. (b) Shultz, D. A.; Boal, A. K.; Farmer, G. T. *J. Org. Chem.* **1998**, *63*, 9462. (c) Shultz, D. A.; Bodnar, S. H. *Inorg. Chem.* **1999**, *38*, 591.

10.1021/ic020520q CCC: $25.00
Published on Web 03/05/2003

as **1**−**3** are attractive radical ligand systems because they

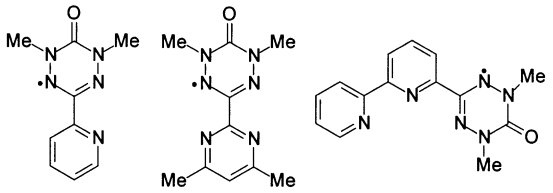

1 **2** **3**

behave as structural mimics of oligopyridines.[8−12] This has allowed control over the structure of the metal−verdazyl complexes, and therefore control over the metal−radical exchange interactions, which, in some cases, can be exceptionally strong.[8,9] In an earlier paper we reported the structure and magnetic properties of a nickel(II) complex of the tridentate verdazyl **3**, a verdazyl-based mimic of the well-known tridentate 2,2′:6′,2″-terpyridine.[9] Herein we present the synthesis and characterization of Mn, Ni, Cu, and Zn complexes of **3**.

Experimental Section

General Information. NMR spectra were recorded on a 300 MHz instrument. Infrared spectra were recorded as KBr pressed pellets. EPR spectra were recorded on a Bruker AMX360 spectrometer, and the spectra so obtained were simulated using the WinEPR SimFonia program. UV−vis spectra were recorded on a Cary 5 spectrophotometer. Elemental analyses were carried out by Canadian Microanalytical Services, Ltd., Vancouver, BC, Canada. 2,2′-Bipyridine-6-carboxaldehyde[13] and carbonic acid bis(methylhydrazide)[14] were prepared according to literature procedures. The preparation of **6** was described previously.[9] All other reagents and solvents were used as purchased. All yields are for recrystallized material.

Caution! Note that perchlorate salts are potentially explosive and must be handled carefully in small quantities as hydrated salts, and never dehydrated under vacuum prior to use.

1,5-Dimethyl-3-(2,2′-bipyridin-6-yl)-1,2,4,5-tetrazane 6-Oxide (4). A solution of 2,2′-bipyridine-6-carboxaldehyde[12] (930 mg, 5.05 mmol) in 150 mL of methanol was added dropwise to a refluxing solution of carbonic acid bis(methylhydrazide) (600 mg, 5.08 mmol) in 20 mL of methanol. After the addition was complete (approximately 2 h), the solution was stirred at reflux for 18 h. The reaction mixture was then cooled to room temperature, and the solvent was removed under reduced pressure, yielding a yellow oil. Ethyl acetate (∼15 mL) was added to the oil, which dissolved with gentle heating. The solution was stored in a freezer for 24 h, affording white needles of **4**, yield 950 mg (66%). ^{1}H NMR (CD_2Cl_2): δ 8.67 (d, 1H, J = 4.4 Hz), 8.45 (d, 1H, J = 8.1 Hz), 8.4 (d, 1H, J = 8.1 Hz), 7.91−7.82 (m, 2H), 7.45 (d, 1H, J = 6.6 Hz), 7.34 (td, 1H, J = 5.9, 1.5 Hz), 5.09 (d, 2H, J = 11.8 Hz), 4.92 (t, 1H, J = 11.8 Hz), 3.13 (s, 6H) ppm. ^{13}C NMR (CD_2Cl_2): δ 156.3, 155.4, 154.9, 153.6, 149.6, 138.6, 137.2, 124.5, 123.8, 121.6, 121.2, 69.8, 38.2 ppm. IR (KBr): 3238(m), 3064(w), 3014(w), 2963(w sh), 2913(w), 2862(w sh), 1636(s sh), 1627(s), 1583(m), 1488(w), 1457(w), 1432(s), 1418(s sh), 1381(s), 1300(w), 1255(w), 1202(w), 1118(m), 1096(w), 1062(w), 995(m), 948(m), 861(m), 825(m), 783(s), 749(w), 718(m), 668(w), 648(m), 632(w), 615(w), 531(m) cm^{-1}. Anal. Calcd for $C_{14}H_{16}N_6O$: C, 59.14; H, 5.67; N, 29.56. Found: C, 58.79; H, 5.66; N, 29.57. MS (CI methane): m/z 285 (M + 1, 100). Mp: 162−163 °C.

1,5-Dimethyl-3-(2,2′-bipyridin-6-yl)-6-oxoverdazyl (3). To a vigorously stirred slurry of **4** (348 mg, 1.2 mmol) in 7.5 mL of water was added dropwise a solution of $NaIO_4$ (391 mg, 1.83 mmol) in 10 mL of water, resulting in complete dissolution of **4** and subsequent formation of a brilliant orange solid. Stirring was continued for 25 min, and then the reaction mixture was cooled in an ice bath for 30 min. The orange product was isolated by vacuum filtration, washed with ∼30 mL of cold distilled water, and air-dried, yield 310 mg (92%). Chromatography of the orange solid results in decomposition of the radical, although enough pure material can be isolated by flash chromatography (SiO_2/CH_3CN eluent) for partial characterization. IR (KBr): 3058(w), 2969(w sh), 2935(w), 1683(s), 1577(m sh), 1560(m), 1465(w), 1432(m), 1376(w sh), 1258(m), 1149(w), 1079(w), 1046(w), 1029(w), 990(w), 827(w), 786(s), 746(m), 716(w sh), 690(m), 668(w), 634(w), 618(w), 534(m). UV−vis (CH_2Cl_2): λ_{max} (ϵ (M^{-1} cm^{-1})) 401 nm (1.1×10^3). MS (FAB positive mode): m/z 282 (M + 1, 100), 253 (M − $2CH_3^+$, 5). Mp: 94 °C dec.

Preparation of Complexes 5, 7, and 8. A slurry of **3** (290 mg scale) in methanol (5−8 mL) and $M(ClO_4)_2 \cdot 6H_2O$ (0.5 equiv for M = Mn(II), Cu(II), and Zn(II)) in water (5 mL) were combined, resulting in dissolution of the ligand and instantaneous solution color changes to deep purple for M = Mn(II) and Zn(II) and very dark green for M = Cu(II). The solutions were concentrated in vacuo, cooled in an ice bath, and filtered. The precipitates were washed with cold water and dried. Well-formed crystals were obtained for **7** and **8** by ether diffusion into a nitromethane solution of the complex. Complex **5** was recrystallized by allowing an approximately 1:2.5 acetonitrile/toluene solution of the complex to stand at room temperature in a closed vial over a 24 h period.

[Mn(bipyvd)$_2$](ClO$_4$)$_2$·H$_2$O (5). Yield: 75%. IR (KBr): 3081(w), 2935(w), 1700(s), 1653(w sh), 1600(m), 1577(m), 1492(w sh), 1460(m), 1439 (w sh), 1404(w sh), 1351(w), 1321(w sh), 1302(w), 1276(m), 1251(w sh), 1146(m sh), 1109(m sh), 1084(s br), 1037(w sh), 1020(w), 1007(w), 831(w), 785(m), 748(w), 710(w), 687(m), 657(w), 626(m), 554(w sh), 542(m) cm^{-1}. Anal. Calcd for $C_{28}N_{12}O_{11}H_{28}Cl_2Mn$: C, 40.30; H, 3.38; N, 20.14. Found: C, 40.57; H, 3.15; N, 20.33. UV−vis (CH_3NO_2): λ_{max} (ϵ (M^{-1} cm^{-1})) 443 nm (4.2×10^3). MS (ES, 9:1 CH_3CN/H_2O): m/z 716 {(M − ClO_4)$^+$, 20}, 625 (25), 309 {(M − $2ClO_4$)$^{2+}$, 65}, 282 (bipyvd + 1, 100).

[Cu(bipyvd)$_2$](ClO$_4$)$_2$ (7). Yield: 60%. IR (KBr): 3111(w sh), 3082(w), 2940(w), 1701(s), 1604(m), 1576(m), 1499(m), 1462(s), 1436(m sh), 1351(w), 1306(m), 1274(m), 1254(w), 1197(w), 1166(w), 1101(s), 1081(s), 1033(m), 1010(m), 836(w), 785(m), 745(w), 717(m), 683(m), 620(s), 538(m) cm^{-1}. Anal. Calcd for

(5) (a) Manriquez, J. M.; Yee, G. T.; MacLean, S.; Epstein, A. J.; Miller, J. S. *Science* **1991**, *252*, 141. (b) Bohm, A.; Vazquez, C.; McLean, R. S.; Calabrese, J. S.; Kalm, S. E.; Manson, J. L.; Epstein, A. J.; Miller, J. S. *Inorg. Chem.* **1996**, *35*, 3083.
(6) Fujita, W.; Awaga, K. *J. Am. Chem. Soc.* **2001**, *123*, 3601.
(7) Neugebauer, F. A. *Angew. Chem., Int. Ed. Engl.* **1973**, *12*, 455. (b) Neugebauer, F. A.; Fischer, H.; Siegel, R. *Chem. Ber.* **1988**, *121*, 815.
(8) Hicks, R. G.; Lemaire, M. T.; Thompson, L. K.; Barclay, T. M. *J. Am. Chem. Soc.* **2000**, *122*, 8077.
(9) Barclay, T. M.; Hicks, R. G.; Lemaire, M. T.; Thompson, L. K. *Chem. Commun.* **2000**, 2141.
(10) Barclay, T. M.; Hicks, R. G.; Lemaire, M. T.; Thompson, L. K. *Inorg. Chem.* **2001**, *40*, 5581.
(11) Brook, D. J. R.; Lynch, V.; Conklin, B.; Fox, M. A. *J. Am. Chem. Soc.* **1997**, *119*, 5155.
(12) Brook, D. J. R.; Fornell, S.; Stevens, J. E.; Noll, B.; Koch, T. H.; Eisfield, W. *Inorg. Chem.* **2000**, *39*, 562.
(13) Heirtzler, F. R.; Neuberger, M.; Zehnder, M.; Constable, E. C. *Liebigs Ann./Recl.* **1997**, 297.
(14) Barr, C. L.; Chase, P. A.; Hicks, R. G.; Lemaire, M. T.; Stevens, C. L. *J. Org. Chem.* **1999**, *64*, 8893.

Table 1. Crystallographic Data for Compounds **5**, **7**, and **8**

	5	**7**	**8**
empirical formula	$C_{28}H_{26}N_{12}O_{10}Cl_2Mn\cdot H_2O$	$C_{28}H_{26}N_{12}O_{10}Cl_2Cu$	$C_{28}H_{26}N_{12}O_{10}Cl_2Zn$
fw	832.45	825.05	826.88
cryst syst	orthorhombic	triclinic	triclinic
cryst size (mm)	0.09 × 0.34 × 0.38	0.04 × 0.38 × 0.55	0.07 × 0.25 × 0.41
T (K)	293(2)	293(2)	293(2)
space group	$Pna2_1$	$P\bar{1}$	$P\bar{1}$
Z	4	2	2
a (Å)	18.755(4)	9.4638(18)	9.4858(14)
b (Å)	11.154(3)	9.8442(19)	9.7919(14)
c (Å)	16.594(4)	18.769(4)	18.889(3)
α (deg)	90.00	103.746(3)	104.196(3)
β (deg)	90.00	92.925(3)	92.855(3)
γ (deg)	90.00	94.869(3)	94.216(3)
V (Å^3)	3471.4(13)	1687.8(6)	1692.1(4)
ρ_{calcd} (g cm^{-3})	1.593	1.62	1.623
μ(Mo Kα) (mm^{-1})	0.612	0.88	0.959
λ (Å)	0.71073	0.71073	0.71073
GOF[a]	0.861	1.00	0.942
R1(F_o),[b] $I > 2\sigma(I)$	0.0710	0.049	0.0357
wR2(F_o),[c] $I > 2\sigma(I)$	0.1029	0.132	0.1431

[a] GOF = $[\sum w(|F_o|^2 - |F_c|^2)2/(n-p)]^{1/2}$. [b] R1($F_o$) = $\sum(|F_o| - |F_c|)/\sum|F_o|$. [c] wR2($F_o$) = $\sum(w^{1/2}|F_o| - |F_c|)/\sum w^{1/2}|F_o|$.

$C_{28}N_{12}O_{10}H_{26}Cl_2Cu$: C, 40.76; H, 3.18; N, 20.37. Found: C, 40.44; H, 3.34; N, 20.04. UV−vis (CH_3NO_2): λ_{max} (ϵ (M^{-1} cm^{-1})) 437 nm (4.3 × 10^3). MS (FAB): *m*/*z* 724 {(M − ClO_4)$^+$, 5}, 625 {(M − ClO_4 − $HClO_4$)$^+$, 25}, 344 {M(bipyvd)$^+$, 100}.

[Zn(bipyvd)$_2$](ClO$_4$)$_2$ (8). Yield: 75%. IR (KBr): 3114(w sh), 3077(w), 2937(w), 2886(w), 1705(s), 1601(m), 1576(m), 1495(w), 1461(w), 1321(w), 1306(w), 1273(m), 1255(w), 1196(w), 1100 + 1085(s doublet), 1026(w sh), 1008(w sh), 831(w), 787(m), 746(w), 708(w), 684(m), 636(w sh), 621(m), 551(w sh), 536(m) cm^{-1}. Anal. Calcd for $C_{28}N_{12}O_{10}H_{26}Cl_2Zn$: C, 40.67; H, 3.17; N, 20.33. Found: C, 40.34; H, 3.33; N, 20.14. UV−vis (CH_3NO_2): λ_{max} (ϵ (M^{-1} cm^{-1})) 438 nm (4.2 × 10^3). MS (ES, 9:1 CH_3CN/H_2O): *m*/*z* 727 {(M − ClO_4)$^+$, 20}, 640 (25), 313 {(M − 2ClO_4)$^{2+}$, 30}, 282 (bipyvd + 1, 100).

X-ray Structure Determinations. Crystal data and details of the data collection for **5**, **7**, and **8** are given in Table 1; the structure of **6** has been reported in ref 8. Data were collected on a Smart 1000 diffractometer (Mo Kα, graphite-monochromated radiation (λ = 0.71073 Å)). Data were collected for 4° < 2θ < 50°. Empirical absorption corrections (SADABS) were applied. The structures were solved by direct methods (SHELXS-97), and the hydrogen atoms were placed at idealized positions and refined according to the riding model. The structures were refined according to the full-matrix least-squares method on F^2 (SHELXL-97). The weighted *R* factor wR2 and goodness of fit *S* are based on F^2; conventional *R* factors R1 are based on *F*.

Magnetic Measurements. Variable-temperature magnetic data (2−300 K) were obtained with a Quantum Design MPMS5S Squid magnetometer operating at 0.1−0.5 T. Calibrations were carried out with a palladium standard cylinder, and temperature errors were determined with [H_2TMEN][$CuCl_4$].[15] Diamagnetic corrections were made using Pascal's constants.

Results

Synthesis. The verdazyl radical **3** was synthesized as shown in Scheme 1. Condensation of 2,2′-bipyridine-6-carboxaldehyde with carbonic acid bis(1-methylhydrazide) afforded the tetrazane **4**. Oxidation of the tetrazane with sodium periodate gave the radical **3** as a deep orange powder in near quantitative yield. Although **3** decomposes slowly in solution, it is persistent enough to allow for its characterization (mass spectrometry, IR, and EPR) and subsequent coordination chemistry. The EPR spectrum of **3** in CH_2Cl_2 (see the Supporting Information) is very similar to that obtained for other N-heterocyclic-substituted verdazyl radicals and is consistent with the spin distribution confined principally to the four verdazyl heterocyclic nitrogen atoms; very little spin density is observed on the bipyridine substitutent.[12,14]

Scheme 1

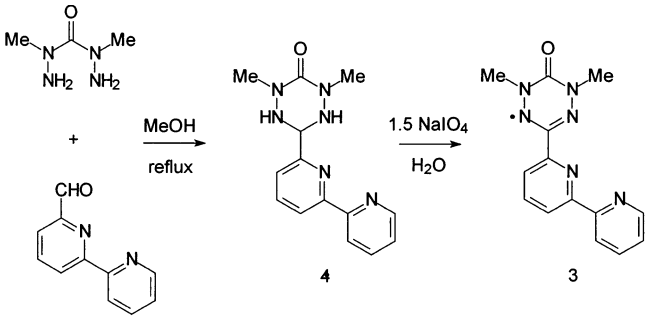

Complexes of **3** were prepared by mixing the radical with metal(II) perchlorate or hexafluorophosphate salts. Precipitation of the complexes and subsequent recrystallization afforded air-stable complexes [M(**3**)$_2$][X]$_2$ (**5**, M = Mn(II); **6**, M = Ni(II); **7**, M = Cu(II); **8**, M = Zn(II); X = ClO_4 for **5**, **7**, and **8** and X = PF_6 for **6**). The solution UV−vis spectra of the four complexes are all very similar to one another and are also qualitatively similar to the spectrum of uncoordinated **3**; the peak maxima are red shifted by ∼40 nm for all complexes (Figure 1). The changes in the visible spectra upon coordination are entirely consistent with previously described transition-metal−verdazyl complexes[8,12,16] and are consistent with the formulation of compounds **5**−**8** as M(II) complexes with coordinated radicals; the perturba-

(15) Brown, D. S.; Crawford, V. H.; Hall, J. W.; Hatfield, W. E. *J. Phys. Chem.* **1977**, *81*, 1303.

(16) Hicks, R. G. *Aust. J. Chem.* **2001**, *54*, 597.

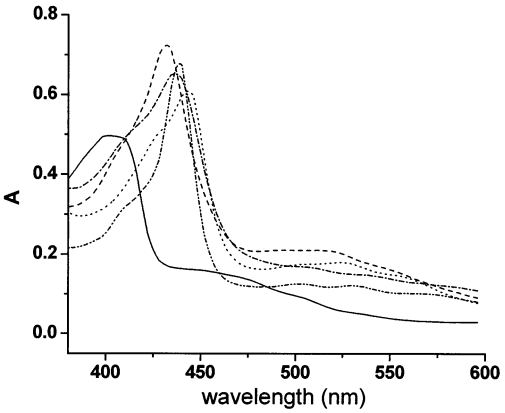

Figure 1. UV−vis spectra of **3** (—), **5** (···), **6** (-··-), **7** (-·-), and **8** (---).

Table 2. Selected Bond Lengths (Å) for **5**, **7**, and **8**

bond	5	7	8
M−N(1)	2.260(5)	2.128(4)	2.155(4)
M−N(2)	2.181(5)	1.962(3)	2.060(4)
M−N(3)	2.252(6)	2.330(4)	2.315(4)
M−N(7)	2.254(6)	2.122(4)	2.150(4)
M−N(8)	2.195(7)	1.970(3)	2.069(4)
M−N(9)	2.316(6)	2.347(4)	2.331(4)
N(9)−N(10)	1.338(8)	1.359(5)	1.362(6)
N(11)−N(12)	1.344(9)	1.366(5)	1.362(6)
N(9)−C(25)	1.348(9)	1.334(5)	1.329(6)
N(12)−C(25)	1.318(9)	1.324(5)	1.331(6)
N(10)−C(27)	1.381(11)	1.395(6)	1.380(7)
N(11)−C(27)	1.405(12)	1.363(6)	1.362(7)
N(10)−C(28)	1.444(9)	1.420(6)	1.425(7)
N(11)−C(26)	1.490(11)	1.477(6)	1.462(7)
C(27)−O(10)	1.219(10)	1.217(6)	1.214(6)

Table 3. Selected Bond Angles (deg) for **5**, **7**, and **8**

angle	5	7	8
N(2)−M−N(8)	164.2(2)	177.5(15)	176.5(16)
N(2)−M−N(3)	71.8(2)	74.83(14)	73.52(15)
N(8)−M−N(3)	123.8(2)	107.02(14)	109.57(15)
N(2)−M−N(7)	105.9(2)	99.14(14)	101.38(16)
N(8)−M−N(7)	73.4(3)	79.25(14)	77.06(16)
N(3)−M−N(7)	92.0(2)	90.46(14)	92.65(15)
N(2)−M−N(1)	72.2(2)	79.2(14)	76.61(15)
N(3)−M−N(9)	98.2(2)	88.32(13)	90.64(14)
N(8)−M−N(1)	92.1(2)	99.22(14)	100.49(15)
N(3)−M−N(1)	143.7(2)	152.61(13)	149.35(15)
N(7)−M−N(1)	94.3(2)	102.21(14)	99.87(16)
N(2)−M−N(9)	111.5(2)	107.31(13)	108.97(15)
N(8)−M−N(9)	71.1(2)	74.58(14)	72.94(15)
N(7)−M−N(9)	142.6(3)	152.19(13)	149.13(15)
N(1)−M−N(9)	98.18(2)	91.22(13)	92.6(15)

tions to the electronic structure of the radical upon coordination are minor.

X-ray Structures. The X-ray crystal structures of complexes **5**−**8** have been determined. All compounds consist of pseudooctahedral (D_{2d} distorted) M(II) ions containing two molecules of **3** bound in the expected tridentate fashion. Tables 2 and 3 summarize selected bond lengths and angles, respectively, for complexes **5**, **7**, and **8**. The general structural features of the verdazyl rings of the coordinated ligands are similar to those of structurally characterized 1,5-dimethyl-6-oxoverdazyls, whether coordinated to a metal or not, although there is a slight asymmetry in the bond lengths and angles induced by coordination to the metal center.[17]

$[Ni(3)_2](PF_6)_2 \cdot C_3H_6O_2$ (6). Structural details for **6** (which crystallizes as an acetone solvate) were reported in an earlier paper.[9] A structural feature of note for **6** is that the two nickel−verdazyl coordinate bonds (2.209 and 2.212 Å) are the smallest observed of the four complexes. Each of the two ligands in **6** are planar and are essentially perpendicular to one another, with an interligand dihedral angle of 92.4°. The angle between the nickel center through the central pyridine nitrogen atoms (N2−Ni−N8) is 175.08°, close to the ideal value; the angle between the ligating verdazyl nitrogen atom and the terminal pyridine nitrogen atom on the same bipyvd ligand through nickel (N9−Ni−N7) is 154.59°.

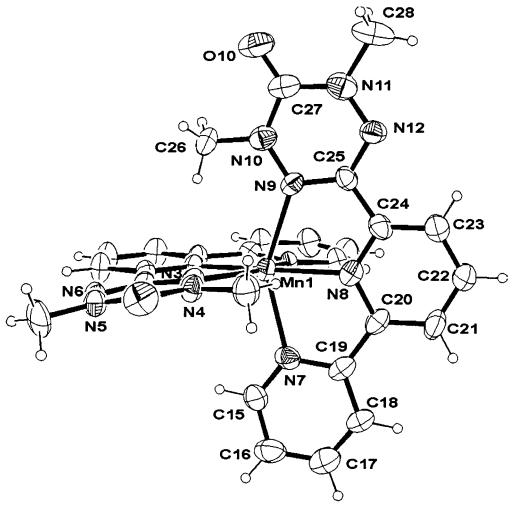

Figure 2. Molecular structure of the dication of **5** (30% probability thermal ellipsoids).

$[Mn(3)_2](ClO_4)_2 \cdot H_2O$ (5). An ORTEP view of the dication of **5** is shown in Figure 2, which crystallizes as a water solvate. The six Mn−N bonds occur in three pairs with a distinct progression of bond lengths—a feature that is shared by all four complexes. The shortest bonds are to the central pyridine nitrogen atoms (N2 and N8, mean bond length 2.187 Å), two slightly longer bonds to the terminal pyridine nitrogen atoms (N1 and N7, 2.257 Å), and two yet longer bonds to the verdazyl ring nitrogen atoms (N3 and N9, 2.284 Å). The coordinate bonds to the nitrogen atoms of the bipyridine fragment of **3** are by far the longest in the manganese structure, with respect to complexes **6**−**8**. The angle between the two central pyridine ring nitrogen atoms through the manganese center (N2−Mn−N8) is 164.22°, significantly distorted from the ideal 180° and the smallest angle observed for the four complexes. The angle between the verdazyl nitrogen atom and terminal pyridine nitrogen atom of the same ligand through the manganese center (N9−Mn−N7) is 142.59°, also the smallest angle of the four complexes. The Mn(II) cation is known to have a larger ionic radius than Ni(II), Cu(II), and Zn(II); the structural evidence indicates that, of the four complexes, **5** is the most distorted from ideal octahedral geometry. A structural feature of **5** that is not shared by the three other complexes is a slight twisting of the verdazyl ring with respect to the bipyridine substituent (Figure 2), with a dihedral angle of 7.7° for N(9)−

(17) Neugebauer, F. A.; Fischer, H.; Krieger, C. *J. Chem. Soc., Perkin Trans.* **1993**, *2*, 535.

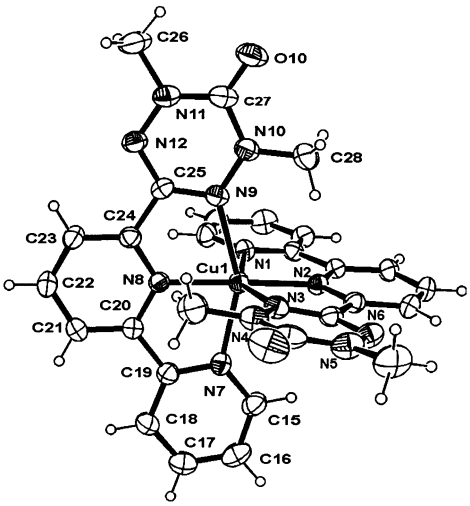

Figure 3. Molecular structure of the dication of **7** (30% probability thermal ellipsoids).

C(25)−C(24)−N(8). Finally, the water molecule in the lattice appears to engage in weak hydrogen bonding with one of the verdazyl carbonyl groups. This interaction is not expected to influence the magnetism of the complex (see below) because the verdazyl oxygen atom has very little spin density.

$[Cu(3)_2](ClO_4)_2$ (7) and $[Zn(3)_2](ClO_4)_2$ (8). An ORTEP view of the dication of **7** is shown in Figure 3. (The ORTEP plot of the dication of **8** can be found in the Supporting Information.) Complexes **6**−**8** exhibit very similar molecular structures, with the two ligands within each complex being nearly planar and perpendicular with one another. An important structural feature of **7** which may have a dramatic effect on its magnetic properties (see below) is the long bonds between the copper center and the verdazyl ring nitrogen atoms (2.347 and 2.330 Å) compared with those observed for **6** (2.209 and 2.212 Å). In the Zn complex **8** the coordinate bonds to the verdazyl nitrogen atoms are slightly shorter than those in **7**, but still significantly larger than those found in **6**. Other intramolecular structural features of **8** are similar to those of **6** and **7**. The Cu−N bond to the terminal pyridine ring (N7) of **7** is similar to that observed for the other three complexes and actually less than that observed for both the zinc and manganese complexes. The coordinate bonds to the central pyridine ring nitrogen atoms, however, are the shortest for the Cu complex with respect to the other three complexes (mean bond length 1.966 Å). This is also observed in the solid-state structures of $[Cu(terpy)_2](NO_3)_2$[18] (1.988 Å) and $[Cu(terpy)_2](PF_6)_2$[19] (1.977 Å), and was rationalized on the basis of a tetragonal compression induced by the influence of the rigid structure of the terpy ligands.[18]

Magnetic Properties. The temperature dependence of molar magnetic susceptibility has been measured from 300 to 2 K for complexes **5**−**8**. The results are displayed in the form of χT versus T plots (Figure 4).

$[Mn(3)_2](ClO_4)_2 \cdot H_2O$ (5). The room temperature (300 K) value of χT for **5** (3.01 emu K mol^{-1}) is less than the expected value (χT = 5.13 emu K mol^{-1}) for uncorrelated spins resulting from one high-spin manganese(II) and two verdazyl radicals (Figure 4). As the temperature is lowered, χT gradually decreases and plateaus between 100 and 20 K, reaching a value of 1.9 emu mol K^{-1}. Below 20 K, χT decreases rapidly; this abrupt decrease is possibly a result of zero-field splitting of the high-spin manganese(II) ground state and/or weak antiferromagnetic intermolecular interactions. The profile of the χT versus T plot suggests an S = 3/2 ground state resulting from simultaneous antiferromagnetic coupling of manganese(II) (S = 5/2) to both verdazyl (S = 1/2) spins. The χT data were fitted using a spin Hamiltonian of the form $\mathbf{H} = -J_{Mn-vd}(\mathbf{S}_{vd1}\mathbf{S}_{Mn} + \mathbf{S}_{vd2}\mathbf{S}_{Mn}) - J_{vd-vd}\mathbf{S}_{vd1}\mathbf{S}_{vd2}$, where $\mathbf{S}_{Mn}$ = 5/2 and $\mathbf{S}_{vd1} = \mathbf{S}_{vd2}$ = 1/2.[20] Our best fit was obtained with the following parameters: J_{Mn-vd} = −93 cm^{-1}, J_{vd-vd} = −10 cm^{-1}, g = 2, TIP (temperature-independent paramagnetism) = 0.00012 cm^3 mol^{-1}, ρ (fraction of paramagnetic impurity) = 0, R = 0.019. An antiferromagnetic intermolecular interaction, zJ' = −1.39 cm^{-1}, was incorporated to help fit the low-temperature data.

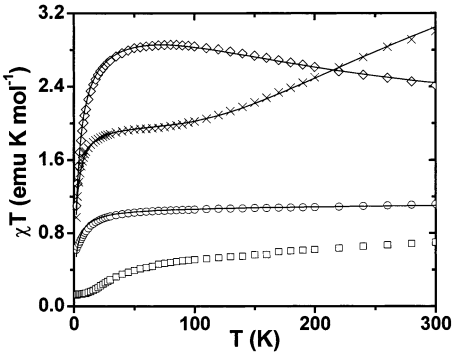

Figure 4. χT vs T plots for **5** (×), **6** (◇), **7** (○), and **8** (□). The solid lines correspond to data fits using the data described in the text.

$[Ni(3)_2](PF_6)_2 \cdot C_3H_6O$ (6). At room temperature, the value of χT (2.42 emu K mol^{-1}) for **6** (Figure 4) is significantly greater than the expected value for three noninteracting spin systems (χT = 1.90 emu K mol^{-1}). As the temperature decreases, χT increases to a maximum value of 2.88 emu K mol^{-1} and then rapidly decreases on further cooling. The high-temperature behavior is strongly indicative of significant ferromagnetic coupling between nickel(II) and verdazyl spins. As with **5**, we fitted the χT data with a three-spin model (with $\mathbf{S}_{Ni}$ = 1 replacing $\mathbf{S}_{Mn}$ = 5/2), but one in which both verdazyl spins are ferromagnetically coupled to a nickel ion ($\mathbf{S}_{Ni}$ = 1) with an exchange parameter J_{Ni-vd}, and interradical interactions are accounted for by another exchange term, J_{vd-vd}. Our best fit gave us the following parameters: J_{Ni-vd} = +240 cm^{-1}, J_{vd-vd} = −8 cm^{-1}, g = 2.02, TIP = 0.0001 cm^3 mol^{-1}, ρ = 0.01, R = 0.035. The abrupt decrease in χT observed at low temperatures could be ascribed either to zero-field splitting of the high-spin ground state of the complex and/or to weak antiferromagnetic interactions. We fit the low-temperature data by arbitrarily incorporating a weak antiferromagnetic interaction zJ' of −2.63 cm^{-1}. Previous analysis of the molecular packing of **6** revealed a possible

(18) Allmann, R.; Henke, W.; Reinen, D. *Inorg. Chem.* **1978**, *17*, 378.
(19) Arriortua, M. I.; Rojo, T.; Amigo, J. M.; Germain, G.; Declercq, J. P. *Acta Crystallogr., Sect. B* **1982**, *B38*, 1323.
(20) Kahn, O. *Molecular Magnetism*; VCH: New York, 1993.

pathway for intermolecular magnetic exchange resulting from overlap of verdazyl rings on adjacent molecules.[9]

$[Cu(3)_2](ClO_4)_2$ (7). At room temperature **7** exhibits a χT value of 1.11 emu K mol^{-1}, which is very close to the expected value (χT = 1.12 emu K mol^{-1}) for three uncorrelated $S = 1/2$ spins. The χT product remains essentially independent of temperature between 300 and 30 K, below which it decreases. The profile of the χT product above 30 K is indicative of Curie−Weiss behavior and negligible intramolecular copper−verdazyl magnetic exchange coupling. The data were modeled by incorporating the same three-spin model that was used with **5** and **6** (but with $\mathbf{S}_{Cu} = 1/2$). The decrease in χT below 30 K is likely due to weak intermolecular antiferromagnetic coupling, and was accounted for by incorporating a weak antiferromagnetic interaction parameter zJ' of −2.79 cm^{-1}. Our best fit was obtained with the following other parameters: $J_{Cu-vd} = -4.5$ cm^{-1}, $J_{vd-vd} = -5$ cm^{-1}, $g_{rad} = 2.00$ (fixed), $g_{Cu} = 2.00$ (fixed), TIP = +0.0001 cm^3 mol^{-1}, $\rho = 0.01$, $R = 0.01$. We note that the model fit below 10 K is not good, indicative of more complex behavior at these very low temperatures.

$[Zn(3)_2](ClO_4)_2$ (8). For the Zn complex, χT at room temperature (0.697 emu K mol^{-1}) is somewhat less than the expected value for two uncorrelated $S = 1/2$ spins (χT = 0.75 emu K mol^{-1}). The steady decrease in χT as the temperature is lowered indicates that weak to moderate antiferromagnetic interactions between coordinated radicals are operative within molecules of **8**. Below 50 K, χT decreases more rapidly and reaches a final value of 0.123 emu K mol^{-1} at 2 K. Qualitatively, the antiferromagnetic exchange seems to be consistent with the intramolecular radical−radical interactions in the other three complexes. However, the magnetic data for the Zn complex could not be fit to a simple two-spin model ($\mathbf{H} = -J(\mathbf{S}_{vd1}\mathbf{S}_{vd2})$), even when using only relatively high temperature data. This suggests the presence of significant intermolecular contributions to the observed magnetic behavior. Attempts to model the data using Weiss-type constants to explicitly account for intermolecular magnetic exchange were fruitless, as were attempts to model the data using 1D or 2D antiferromagnetic chains. Analysis of the crystal packing in **8** does not reveal any close intermolecular contacts—and particularly none involving the verdazyl nitrogen atoms bearing substantial spin density—that could provide apparent intermolecular exchange pathways. The slight upturn in the χT vs T plot for **8** at very low temperatures prompted us to study the field dependence of the magnetization for this complex, but no evidence for ordering was found. Moreover, the value of the saturation magnetization corresponds to 1/3 of an electron. Clearly the magnetic properties of this complex are unusual and require further studies.

Discussion

The coordination chemistry of oligopyridine-type chelating ligands, such as bipyridine and terpyridine, is extensive.[21] Judiciously substituted verdazyl radicals are structural mimics of the oligopyridine family of ligands; in the present case **3** presents a chelating environment that is identical to that of terpy. Using this structural analogy as a tool, we can control the structures of the metal−verdazyl complexes, and this should allow us to exhibit similar influences over the magnetic behavior. On the basis of our previous work with mono- and binuclear $M(hfac)_2$ complexes [M = Ni(II) and Mn(II)] with pyridine- and pyrimidine-substituted verdazyl radicals (**1** and **2**, respectively), in concert with well-established orbital symmetry arguments,[8,10,16,22] we could predict the magnetic behavior of our 2:1 complexes with **3**, particularly for **5** and **6**.

Structurally, the local features of the metal complexes **5**−**8** were similar to those of the corresponding $M(terpy)_2^{2+}$ complexes described in the literature[21]—further validating our oligopyridine−verdazyl structural analogy. The Mn−verdazyl binding features in **5** are also similar to those of other manganese(II) verdazyl complexes that we have prepared, and all three complexes exhibit very similar magnetic behavior. Previously we rationalized the magnetic behavior of the Mn complexes of **1** and **2** on the basis of $d\pi-p\pi$ overlap between the verdazyl SOMO (a π symmetry orbital spanning the four nitrogens of the verdazyl ring) and two of the metal-centered t_{2g} orbitals.[8,10] The magnetic data obtained for **5** indicate that these symmetry arguments can be generalized to pseudooctahedral manganese(II) verdazyl complexes, even those with disparate ancillary ligand sets.

The very strong intramolecular ferromagnetic coupling demonstrated by **6** (J_{Ni-vd} = +240 cm^{-1}) can also be explained using orbital symmetry arguments. The molecular structure of **6** is very similar to that found in $Ni(terpy)_2^{2+}$ complexes.[23] Thus, the SOMO of the coordinated radical is strictly orthogonal to the two unpaired spins in the e_g set of nickel(II) orbitals, resulting in ferromagnetic coupling—exactly what was observed in a Ni(II) complex of **1**.[8] On the basis of this result, and because copper(II) is a d^9 system with the unpaired electron housed in one of the e_g orbitals that cannot overlap with the verdazyl SOMO, we expected **7** to also exhibit intramolecular ferromagnetic copper−verdazyl exchange coupling. However, the magnetic data indicate that only very weak antiferromagnetic intramolecular coupling occurs in **7**. The reason for this may be in part due to the very long copper−verdazyl nitrogen atom coordinate bonds (2.35 Å). The longer distances between spin-bearing atoms apparently weaken the exchange interactions between Cu(II) and the radicals. However, it is difficult to assess whether the degree of metal−verdazyl bond lengthening in **7** vs **6** is sufficient to produce the observed changes in magnetic exchange behavior. To test this hypothesis, more Cu(II) complexes of verdazyl radicals (ideally with a range of Cu−N bond lengths) are required. Efforts to this end are in progress.

The zinc(II) analogue **8** was prepared to more accurately determine the sign and magnitude of intramolecular radical−radical coupling that is operative in these complexes; because

(21) Constable, E. C. *Adv. Inorg. Chem. Radiochem.* **1986**, *30*, 69. (b) Constable, E. C. *Adv. Inorg. Chem. Radiochem.* **1989**, *34*, 1.
(22) Kahn, O.; Prins, R.; Reedijk, J.; Thompson, J. S. *Inorg. Chem.* **1987**, *26*, 3557.
(23) Constable, E. C.; Lewis, J.; Liptrot, M. C.; Raithby, P. R. *Inorg. Chim. Acta* **1990**, *178*, 47.

Zn(II) is diamagnetic, the major contribution to the susceptibility in **8** should in principle arise from radical−radical coupling. Unfortunately it appears that intermolecular effects strongly contribute to, and may even dominate, the susceptibility profile for complex **8**. We have observed fairly strong intermolecular exchange interactions in structurally characterized free (uncomplexed) verdazyl radicals,[24] and these interactions may have to be factored more explicitly into analyses of the metal complexes of these radicals as well.

Conclusion

We have prepared a novel tridentate bipyridine-substituted verdazyl radical and have structurally and magnetically characterized its manganese(II), nickel(II), copper(II), and zinc(II) complexes. Significantly, the molecular structures of complexes **5**−**8** are analogous to those of $M(terpy)_2^{2+}$ complexes reported in the literature—further validating the oligopyridine−verdazyl structural link we established with previous metal−verdazyl complexes.[8,10] Furthermore, it appears that the magnetic properties of the metal complexes are dependent on the metal ion and the geometry of the complex—and, to a first approximation, independent of the ancillary ligands, as witnessed by the similarity in exchange coupling in complexes with hfac- or pyridine-based ligands. Intermolecular interactions, however, can greatly complicate matters as we have described above. Collectively, these observations provide further stimuli for the synthesis of more exotic verdazyl ligands that are capable of assembly into coordination arrays and polymers with interesting magnetic properties.

Acknowledgment. We thank the Natural Sciences and Engineering Research Council of Canada for financial support of this research in the form of Research and Equipment Grants (R.G.H., L.K.T.) and a Postgraduate Scholarship (M.T.L.).

Supporting Information Available: EPR spectrum of **3**, ORTEP drawing of **8**, and details of the crystal structures of **5**, **7**, and **8** (CIF format). This material is available free of charge via the Internet at http://pubs.acs.org.

IC020520Q

(24) Hicks, R. G.; Lemaire, M. T.; Öhrström, L.; Richardson, J. F.; Thompson, L. K.; Xu, Z. *J. Am. Chem. Soc.* **2001**, *123*, 7154.